Supplementary Information

Title: DNA hydrogel-based supercapacitors operating in physiological fluids

Jaehyun Hur[1], Kyuhyun Im[1], Sekyu Hwang[2], ByoungLyong Choi[1], Sungjee Kim[2], Sungwoo Hwang[1], Nokyoung Park[*1] and Kinam Kim[3]

[1]Frontier Research Laboratory, Samsung Advanced Institute of Technology, Samsung Electronics, Yongin, Kyunggi-do 446-712, South Korea

[2]Department of Chemistry, Pohang University of Science & Technology, Pohang, 790-784, South Korea

[3]Samsung Advanced Institute of Technology, Samsung Electronics, Yongin, Kyunggi-do 446-712, South Korea

[*]Correspondence should be addressed to Nokyoung Park (n2010.park@samsung.com)

S1. Comparison of deposition methods and porous templates

To justify the effectiveness of our deposition process, we compared the electrochemical performances between LBL-prepared electrode and simple dipping-prepared electrode. As shown in Fig S1a and S1b, the specific capacitance is almost double for LBL-prepared electrode, suggesting that the presence of positively-charged PDADMAC promotes the more uniform deposition of conductive PEDOT:PSS. Also, the comparison of electrochemical performances between Dgel and agarose gel indicates the superiority of Dgel template to agarose gel, which is probably due to the contribution of electrostatic interaction between both interfaces of Dgel-PDADMAC and PDADMAC-PEDOT:PSS.

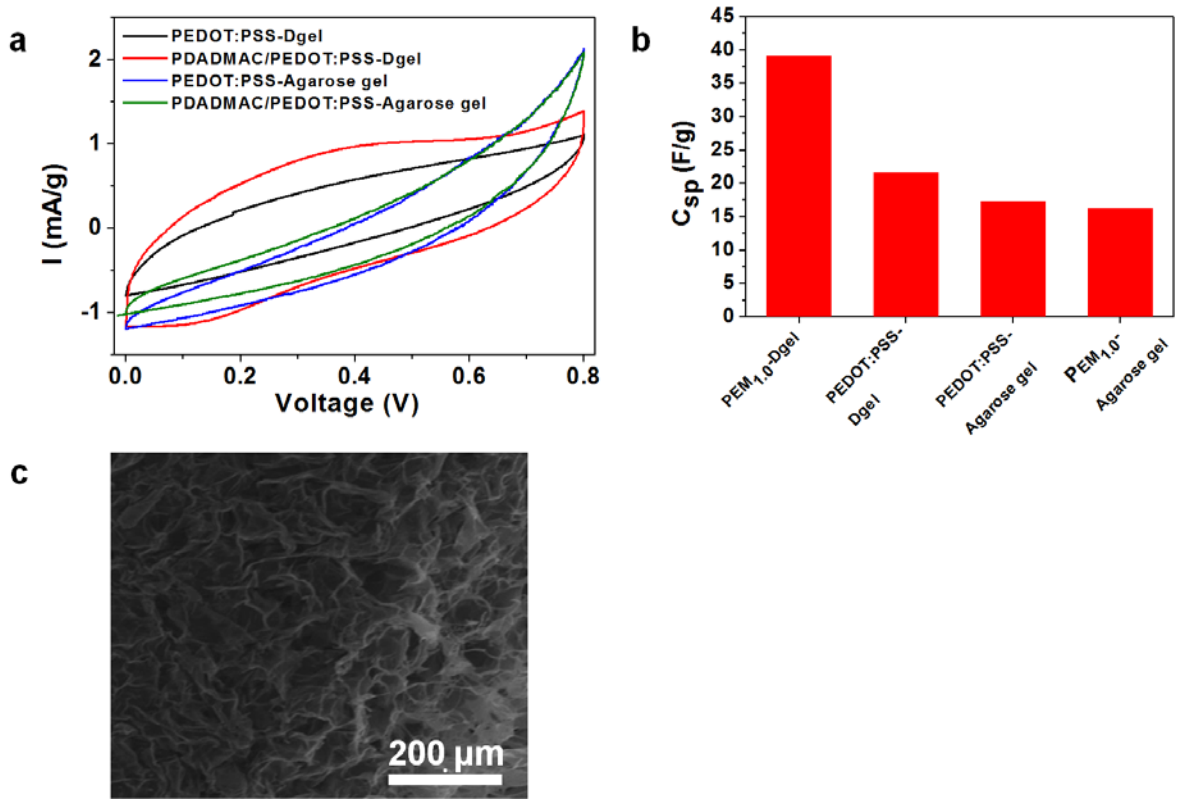

Figure S1. Comparison of specific capacitances between LBL and simple dipping process, and between DNA gel (Dgel) and agarose gel template: **a**, Cyclic voltammograms for PEDOT:PSS-Dgel, $PEM_{1.0}$-Dgel, PEDOT:PSS-agarose gel, and $PEM_{1.0}$-agarose gel. **b**, Specific capacitances calculated from (a), respectively. **c**, SEM image of agarose gel.

S2. Evolution of microscopic morphology for PEM_n-Dgel (n=1.0-5.0)

Fig. S2 presents the morphological change for different number of PEM (from $PEM_{1.0}$ to $PEM_{5.0}$) on Dgel. It can be supposed that if the LBL process was performed suitably, layered structure can be preserved such that each layer maintains its original structure. Indeed, as seen in Fig. S2, the layered Dgel structure is well-preserved even if the number of PEM increases up to five.

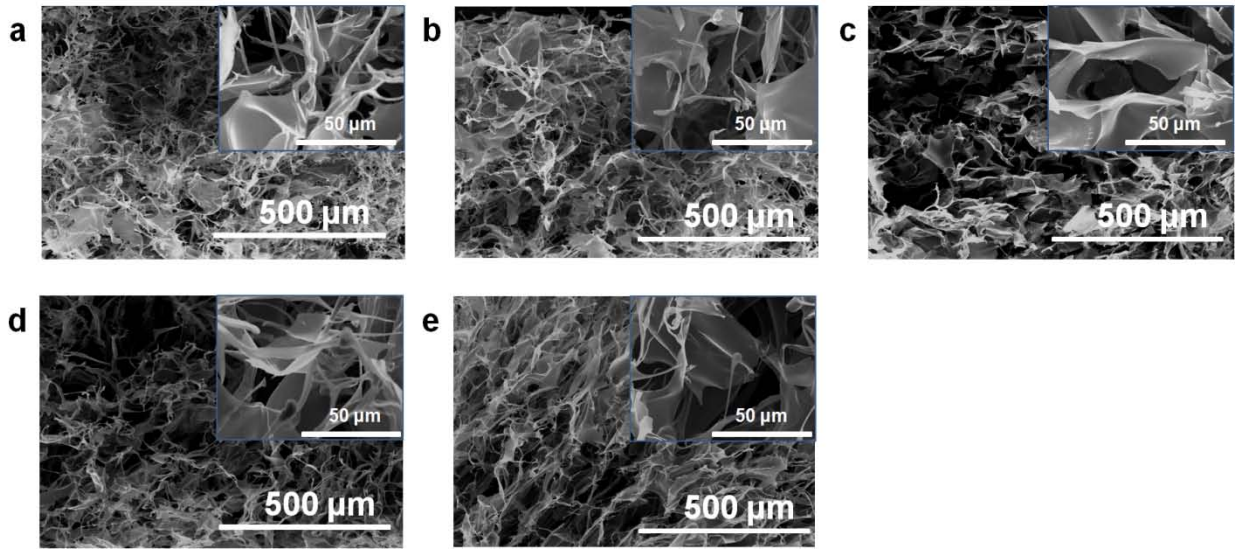

Figure S2. SEM images for PEM-Dgel with **a,** 1 layer, **b,** 2 layers, **c,** 3 layers, **d,** 4 layers, and **e,** 5 layers of PEM. Insets show the enlarged morphological view from each image.

S3. Cytotoxic test of device with HDF and COS7 cell line

In addition to NIH3T3 cells, HDF and COS7 cells were also tested for cytotoxicity of PEM-Dgel supercapacitor during the charge-discharge process. As shown in Fig S3a and S3b, both cells remain intact at the 1,000 charge-discharge cycling processes when pre-cleaning processes were applied.

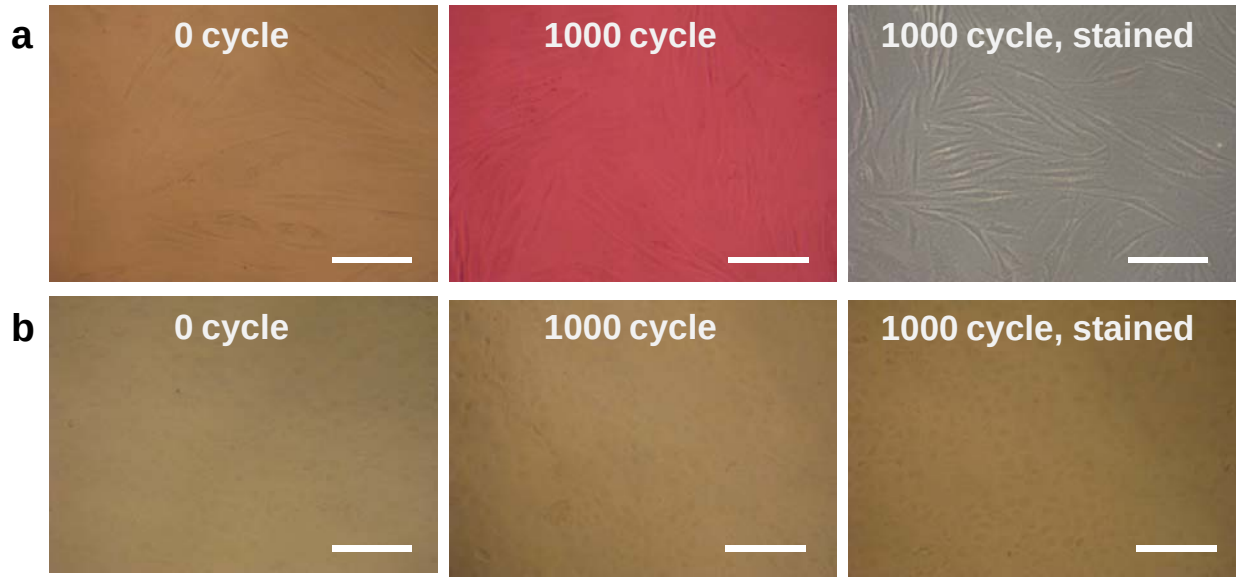

Figure S3. Optical microscopic images of a, HDF cells and b, COS7 cells that underwent the 0 cycle (left), 1000 cycles (middle), and 1000 cycles stained by trypan blue (right). Scale bar: 100 µm.

S4. Galvanostatic charge-discharge measurement for PEM-Dgel in a cell medium

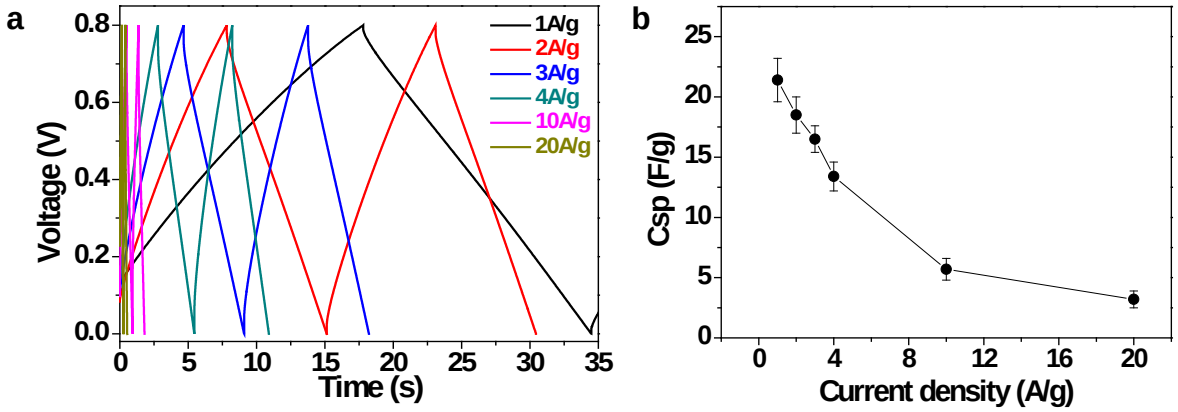

Figure S4. **a,** Charge-discharge plot for PEM-Dgel in a cell medium, **b,** specific capacitance as a function of current density.

S5. Internal resistances for PEM_n-Dgel (n=1.0-5.0) and $PEM_{5.0}/Mn_3O_4$-Dgel

Internal resistances of electrodes measured from charge-discharge curve almost linearly decrease as the number of PEM increases. The increase in conductive layer thickness for higher number of PEM is associated with this resistance decrease. The slight increase of internal resistance in Mn_3O_4 coated PEM results from the relatively higher electric resistance of Mn_3O_4 than that of PEDOT:PSS.

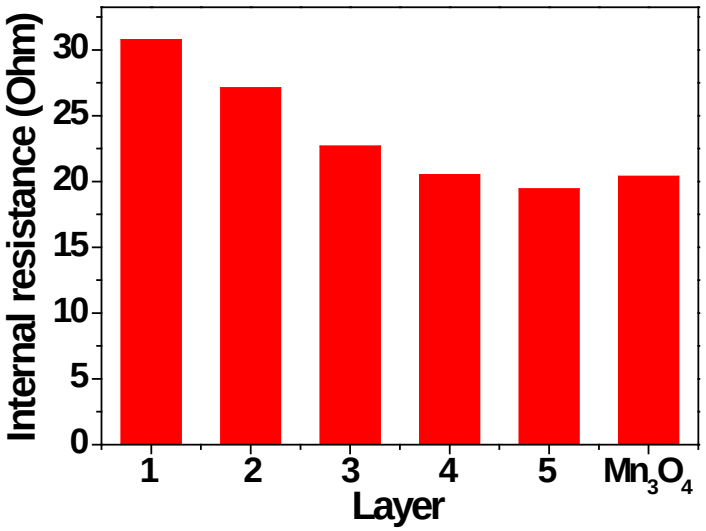

Figure S5. Internal resistance for PEM_n-Dgel (n=1.0-5.0) and $PEM_{5.0}/Mn_3O_4$-Dgel in a 1.0 M H_2SO_4 electrolyte solution at discharge current density at 2.0A/g. The values are calculated from IR drop in galvanostatic charge-discharge measurements.

S6. Supercapacitor performances optimization for PEM_n-Dgel (n=1-5) by the galvanostatic measurments

Regarding the effect of different number of PEM, again, the saturation behavior of discharging time is observed when the number of PEM is over three (Fig. S6b inset). The specific capacitance of ~58.3 F/g for $PEM_{5.0}$-Dgel at 1.0 A/g is not far different from the specific capacitance value of 55.3 F/g for $PEM_{3.0}$-Dgel. When the specific capacity is plotted as a function of different current densities (Fig. S6b), the capacitance increase is significantly suppressed at high current densities (> 10 A/g) even if the number of PEM increases. In this case, for the similar reason in CV data for different number of PEM, the effective contribution of conductive material buildup for higher number of PEM becomes almost negligible.

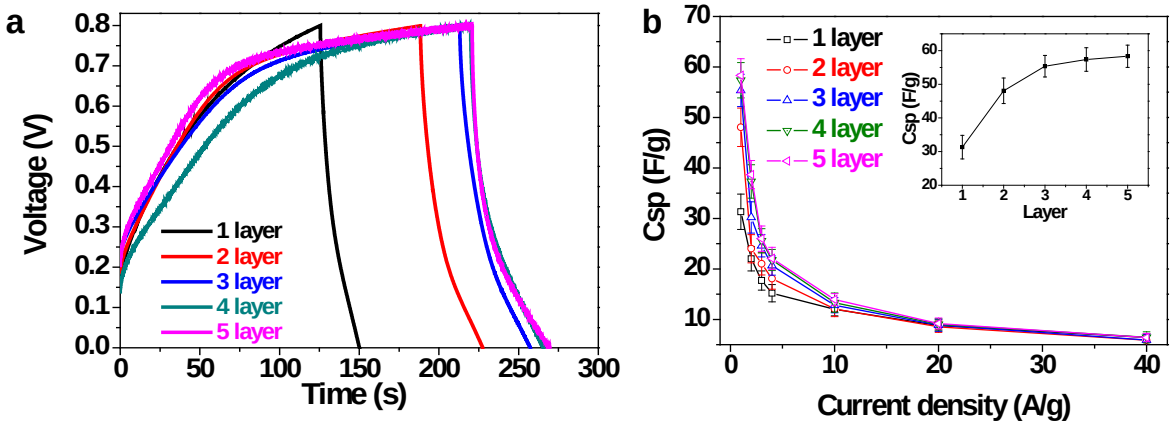

Figure S6. **a,** Charge-discharge plot for PEM_n-Dgel (n=1-5) in H_2SO_4 electrolyte, **b,** specific capacitance as a function of current density. Loading of active material is 0.4, 0.8, 1.2, 1.6, and 2.0 mg/cm^2 for PEM_n-Dgel (n=1-5), respectively.

S7. Ragone plot for PEM_n-Dgel (n=1-5), and $PEM_{5.0}/Mn_3O_4$-Dgel

As shown in Ragone plot for 1-5 layers of PEM-Dgel and $PEM_{5.0}/Mn_3O_4$-Dgel (Fig. S6), the power density and energy density linearly increase simultaneously as the number of PEM increases. The power density of 5198.2 W/kg for $PEM_{1.0}$-Dgel reaches as high as 8230.5W/kg for $PEM_{5.0}$-Dgel. Also, energy density is increased from 1.4 Wh/kg to 2.1 Wh/kg as the number of PEM increases from 1 to 5. For $PEM_{5.0}/Mn_3O_4$-Dgel, the energy density becomes even higher than that of $PEM_{5.0}$-Dgel due to the specific capacitance increase, although the power density stays a similar value to that of $PEM_{5.0}$-Dgel. The increase in power and energy density for more number of PEM is originated from the decrease of internal resistance as the number of PEM increases (Fig. S7). Overall, the power and energy density of our simple device outperforms the commercially available supercapacitors (within the trapezoid in Fig. S7).

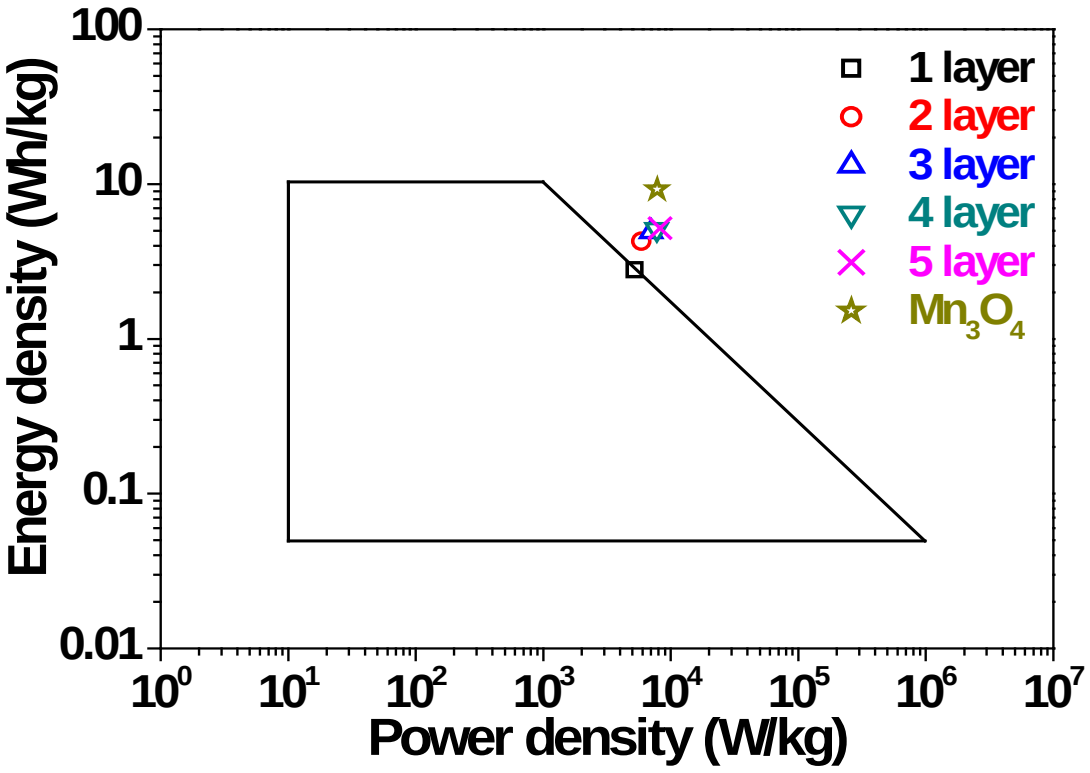

Figure S7. Ragone plot for PEM_n-Dgel (n=1-5), and $PEM_{5.0}/Mn_3O_4$-Dgel. Loading of active material is 0.4, 0.8, 1.2, 1.6, 2.0, and 2.2 mg/cm^2 for PEM_n-Dgel (n=1-5), and $PEM_{5.0}/Mn_3O_4$-Dgel, respectively. Trapezoid indicates the power and energy density range of commercially available supercapacitors.

S8. Characterization of pseudocapacitance Mn_3O_4 and performances improvement

Electrochemical performances of PEM-Dgel have been further improved by employing pseudocapacitance material. Fig. S8a shows that the outer layer of PEM-Dgel has been coated with manganese oxide which is one of the most widely used pseudocapacitance materials owing to its great performances and low price. Manganese oxide has been coated on PEM layer by electroless plating where $KMnO_4$ precursor is reduced to manganese oxide particles on PEM-Dgel. The formation of manganese oxide particles is clearly visible from the observation of solution color change from purple to brown during the reducing step with ammonium hydroxide hydrogen chloride, while the overall layered morphology of PEM-Dgel is maintained. Phase analysis of manganese oxide has been carried out by XRD (Fig. S8b). The peak positions associated with the manganese oxide can be indexed to the tetragonal Mn_3O_4 (hausmannite, space group: I41/amd) with lattice constants of a = b = 5.76 Å and c = 9.47 Å, which are in good agreement with the values given in the standard card for Mn_3O_4 (JCPDS No. 24-0734)[26-29]. In addition, no diffraction peaks of any other phases are detected implying the high purity of the products. The existence of Mn_3O_4 on PEM-Dgel is also confirmed by Raman spectroscopy by comparing the peaks from pure Mn_3O_4 and Mn_3O_4–coated PEM-Dgel (PEM/Mn_3O_4-Dgel) (Fig. S8e)[23-26]. As a result, the specific capacitance of the $PEM_{5.0}$/ Mn_3O_4-Dgel is 99.5 F/g which is 1.7

fold higher than that of $PEM_{5.0}$-Dgel at 25 mV/s scan rate. The increased capacitance is due to charge transfer redox reaction of Mn_3O_4. As shown in Fig. S8c, no Faradaic reaction peak was observed within the voltage scan range (0.0~0.8 V) for $PEM_{5.0}$-Dgel which implies that purely electric double layer (EDL) comes into play, whereas, for $PEM_{5.0}/Mn_3O_4$-Dgel, the redox peaks at ~0.21 and ~0.51 V are observed indicating the charge transfer reaction. The increase of specific capacitance is also confirmed in Fig. S8d where the maximum specific capacitance reaches up to 105.4 F/g for $PEM_{5.0}/Mn_3O_4$-Dgel which is 1.8-fold higher than that of $PEM_{5.0}$-Dgel.

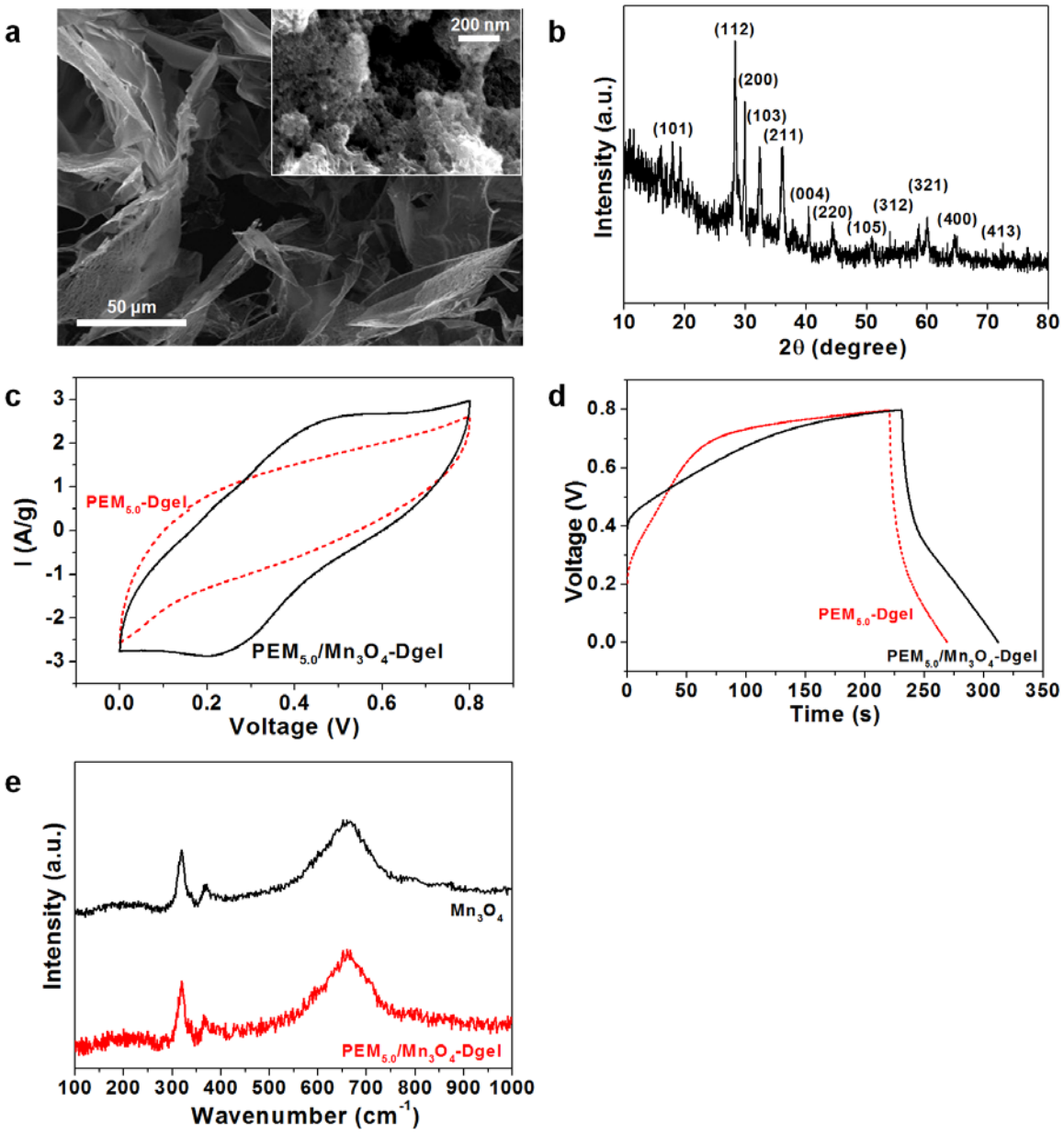

Figure S8. a, SEM image of manganese oxide on PEM-Dgel (inset show the magnified view of Mn_3O_4 particles), **b**, XRD patterns of Mn_3O_4, **c**, Cyclo voltammograms of $PEM_{5.0}$-Dgel (dotted line) and $PEM_{5.0}/Mn_3O_4$-Dgel (solid line) at 25mV/s, **d**, Charge-discharge curves between $PEM_{5.0}$-Dgel (dotted line) and $PEM_{5.0}/Mn_3O_4$-Dgel (solid line), and **e**, Raman spectrum of Mn_3O_4(black line) and $PEM_{5.0}/Mn_3O_4$-Dgel (red line).